pneumonia are often due to bacterial infection. In the case of the influenza pandemic that occurred in 2009, the virus, designated A(H1N1)pdm09, infected pneumocytes in some patients. It also caused severe respiratory failure, similar to that seen for H5N1 infection, during the first year of the outbreak.[22–26] The analysis of 20 autopsied A(H1N1)pdm09 infection cases in Japan revealed that diffuse alveolar damage, similar to that seen in a case of H5N1 infection, was present in the lungs of 5 cases (25%).[27]

The pathological study of human tissues can be restricted because of the difficulty in obtaining samples, but it is crucial for elucidating pathogenesis of the disease. There have been only 16 reports of pathological studies carried out on fatal cases of H5N1 infection. These have been reported from Hong Kong,[3–6] Thailand,[7–13] China[14–17] and Vietnam.[18] Lungs infected with H5N1 presented with diffuse alveolar damage in all cases. In most cases, H5N1 antigens and RNA were detected in extrapulmonary organs, suggesting disseminated systemic H5N1 infection and viremia.

Nearly 77% (10/13 patients) of H5N1 infection cases have resulted in death at the National Hospital of Pediatrics Hanoi, since December 2003. In this study, post-mortem biopsied or autopsied tissues from five fatal cases were analyzed pathologically to reveal virus distribution and the expression levels of cytokines and chemokines in lungs. Immunohistochemistry, *in situ* hybridization, double immunofluorescence staining and quantitative reverse transcription PCR (qRT-PCR) methods were used in our studies.

Materials and methods

Patients and Formalin-Fixed, Paraffin-Embedded Tissues

H5N1 infection of the five cases was confirmed by detecting viral RNA in bronchiolar aspirate using RT-PCR. The numbering of the case was in order of the shortness of the disease duration. In three cases (cases 1, 4 and 5; Table 1), post-mortem biopsied lung tissues were examined; these cases have been reported previously in a short communication.[18] In the other two cases, patients were autopsied at National Hospital of Pediatrics; in addition to lung tissue, liver, heart, kidney, intestine, spleen and pancreas were examined in case 2. For case 3, liver, heart and kidney tissue were also examined in addition to lung tissue (Table 1). Only formalin-fixed, paraffin-embedded tissues were available for this study. This study was approved by the institutional medical ethical committee of the National Institute of Infectious Diseases, Japan (approval no. 320) and National Hospital of Pediatrics Hanoi.

Histopathological Studies and Immunohistochemistry

The formalin-fixed, paraffin-embedded tissues were cut (3-μm thick sections) and mounted on silane-coated glass slides. Histopathological studies were performed on all samples using hematoxylin–eosin (HE) staining. For lung sections, Elastica–Masson Goldner staining was also done. Immunohistochemistry for influenza A nucleoprotein antigen (InfA-NP) was performed to evaluate the distribution of H5N1 antigens with a mouse monoclonal antibody against InfA-NP[28] as previously described.[18,23,27]

Immunohistochemistry for cell type-specific marker proteins, cytokines and chemokines was performed using primary antibodies against the following proteins: myeloperoxidase (MPO; Nichirei Bioscience, Tokyo, Japan); neutrophil elastase (DAKO Cytomation, Copenhagen, Denmark); CD68 (KP-1 or PGM-1; DAKO); CD8 (Novocastra Laboratories, Newcastle, UK); tumor necrosis factor-alpha (TNF-α; BD Pharmingen, San Diego, CA, USA); interleukin (IL)-6 (R&D Systems, Minneapolis, MN, USA); IL-8 (R&D Systems); regulated on activation normal T-cell expressed and secreted (RANTES; R&D Systems); and interferon-gamma-inducible protein of 10 kDa (IP-10; R&D Systems). After incubation with these primary antibodies, signals were detected using the avidin–biotin complex immunoperoxidase method (LSAB2, DAKO). A biotin-free catalyzed signal amplification system (CSAII, DAKO) was used for the detection of TNF-α, IL-6 and CD8. The EnVision system (DAKO) was used for the detection of neutrophil elastase. As a negative control, an irrelevant antibody was used in place of the primary antibody.

In Situ Hybridization

Influenza virus genomic RNA and mRNA were detected in formalin-fixed, paraffin-embedded lung sections by *in situ* hybridization AT tailing combined with a catalyzed signal amplification method (ISH-AT) as described previously.[29,30] Anti-sense and sense ISH-AT probes against H5N1 nucleoprotein (NP) genes were prepared and used to detect H5N1 mRNA and genomic RNA. The anti-sense ISH-AT probe against the rabies virus NP gene was used as an irrelevant negative control (Table 2).

Double Immunofluorescence Staining

Double immunofluorescence staining for InfA-NP, cytokines, chemokines or for cell type-specific marker proteins was performed. We used antibodies against the following marker proteins to determine cell type: MPO (DAKO); surfactant apoprotein D (SP-D; Chemicon, Temecula, CA, USA); CD68 (KP-1 or PGM-1; DAKO); cytokeratin AE1/AE3 (DAKO); epithelial membrane antigen (EMA; DAKO); and CD34 (Novocastra). AlexaFluor 488-conjugated anti-

Table 1 Summary of the five H5N1 infection cases examined in this study

Case	*Date of admission (month, year)*	*Age (year)/ sex*	*Duration of illness (days)*	*Day of admission*	*Sample examined*	*Lung histology*	*Laboratory data (on admission)*			*Treatment*			*Detection of viral-RNA or antigen*			
													qRT-PCR			
							WBC (/mm^3)	*Plt (/mm^3)*	*CRP (mg/dl)*	*Antibiotics*	*Oseltamivir*	*MSL*	*Bronchial aspirate*	*FFPE lung copies per cell*	*IHC*	*ISH*
1	December, 2003	12/F	8	Day 6	Lung	DAD (exudative phase)	2100	45 000	3.1	Yes	No	Yes	+	256	+	+
2	March, 2008	11/M	10	Day 7	Lung, liver, heart, kidney, spleen, intestine, pancreas	DAD (exudative phase)	1700	207 000	6.8	Yes	Yes	Yes	+	4.89	+	+
3	December, 2007	4/M	13	Day 11	Lung, liver, heart, kidney	DAD (exudative phase)	2300	154 000	2.4	Yes	Yes	Yes	+	23.1	+	+
4	July, 2004	4/M	16	Day 8	Lung	DAD (proliferation phase)	2300	150 000	0.59	Yes	Yes	Yes	+	1.05	−	−
5	December, 2003	5/M	18	Day 8	Lung	DAD (proliferation phase)	3400	174 000	0.59	Yes	No	Yes	+	UDL	−	−

Abbreviations: CRP, C-reactive protein; DAD, diffuse alveolar damage; FFPE, formalin-fixed, paraffin-embedded; IHC, immunohistochemistry; ISH, *in situ* hybridization; MSL, methylpredonisolone(10 mg/kg/day); Plt, Platelet; qRT-PCR, quantitaive real-time RT-PCR; UDL, under detection limit; WBC, white blood cell; +, positive; −, negative.

Table 2 Primers and probes for quantitative real-time RT-PCR and *in situ* hybridization AT tailing

Target	*Primer and probe*	*Sequence*	*Gene bank or reference*
Influenza virus-matrix	Forward primer	5′-AGCAAAAGCAGGTAGATRTT-3′	CY006300
	Reverse primer	5′-TCGGCTTTGAGGGGG-3′	Ref. Ng *et al*[31]
	Probe	5′-FAM-AMCCGAGGTCGAAACGTAYG-TAMRA-3′	
TNF-α	Forward primer	5′-CAGAGGGAAGAGTTCCCCAGG-3′	NM_000594.2
	Reverse primer	5′-GGCTACAGGCTTGTCACTGG-3′	
	Probe	5′-FAM-TGGCCCAGGCAGTCAGATCATCTTCTCG-TAMRA-3′	
IL-6	Forward primer	5′-GAAGCTCTATCTCCCCTCCAGG-3′	NM_000600.3
	Reverse primer	5′-GCAACACCAGGAGCAGCC-3′	
	Probe	5′-FAM-ACTCCTTCTCCACAAGCGCCTTCGGT-TAMRA-3′	
IL-8	Forward primer	5′-CTTGGCAGCCTTCCTGATTTC-3′	NM_000584.2
	Reverse primer	5′-GCACTGACATCTAAGTTCTTTAGCA-3′	
	Probe	5′-FAM-GCTCTGTGTGAAGGTGCAGTTTTGCCA-TAMRA-3′	
RANTES	Forward primer	5′-GCATCTGCCTCCCCATATTCC-3′	NM_002985.2
	Reverse primer	5′-CCACTGGTGTAGAAATACTCCTTGA-3′	
	Probe	5′-FAM-CTGCTTTGCCTACATTGCCCGCCCA-TAMRA-3′	
IP-10	Forward primer	5′-GCCATTCTGATTTGCTGCCTTA-3′	NM_001565
	Reverse primer	5′-TGCAGGTACAGCGTACAGTTC-3′	
	Probe	5′-FAM-AGTGGCATTCAAGGAGTACCTCTCTCT-TAMRA-3′	
β-Actin	Forward primer	5′-TGAGCGCGGCTACAGCTT-3′	NM_00110
	Reverse primer	5′-TCCTTAATGTTCACGCACGATTT-3′	Ref. Krafft *et al*[32]
	Probe	5′-FAM-ACCACCACGGCCGAGCGG-TAMRA-3′	
H5N1 virus -NP	Sense probe	5′-GCAAGGGTCAACTCTCCCGAGGAGATCTGGAGCTGCTGGT-$(AT)_{10}$-3′	AY651530
	Antisense probe	5′-ACCAGCAGCTCCAGATCTCCTCGGGAGAGTTGACCCTTGC-$(AT)_{10}$-3′	
Rabies virus -NP	Antisense probe	5′-CAGTGGGGTCCCTTGTCAGCTCCATACCTCCCGTCAGAGC-$(AT)_{10}$-3′	AB573762.1

rabbit or anti-mouse IgG (Molecular Probes) and AlexaFluor 568-conjugated anti-mouse or anti-rabbit IgG (Molecular Probes) were used as secondary antibodies. Nuclei were stained with TO-PRO-3, a specific nucleic acid stain (Molecular Probes). Confocal laser scanning microscopy was used to visualize double immunofluorescence staining as described previously.[18,23,27]

RNA Extraction

RNA was extracted from formalin-fixed, paraffin-embedded tissue sections (10μm × 3) using a Pure-Link FFPE total RNA isolation kit (Invitrogen, Carlsbad, CA, USA) according to the manufacturer's protocol. Each sample was treated with DNase I to eliminate DNA contamination using a Turbo DNA-free kit (Ambion, Austin, TX, USA). The total RNA concentration was determined from spectrophotometric optical density measurements.

qRT-PCR Assays

Copy numbers for each RNA of interest and human β-actin mRNA from each sample were determined by qRT-PCR performed in a Mx3005P (Stratagene, La Jolla, CA, USA) using a QuantiTect Probe RT-PCR kit (Qiagen GmbH, Hilden, Germany). Human β-actin mRNA was used as an internal reference gene that provided a normalization factor for the amount of RNA isolated from a specimen. The copy numbers of H5N1 per cell were calculated using β-actin mRNA copy number, which was estimated to be 1500 copies per cell. For H5N1 RNA, we used a primer-probe set that amplified a segment within the matrix protein (M) region of H5N1 RNA. The RT-PCR thermal cycling conditions were 50 °C for 30 min, then 95 °C for 15 min, followed by 40 cycles of 94 °C for 15 s, and 60 °C for 1 min. All samples were run in triplicate. Primers and probes were synthesized by Sigma Genosys (Sigma-Aldrich, St Louis, MO, USA; Table 2).

Results

Patients

The characteristics of the five patients are presented in Table 1. H5N1 infection was confirmed by detecting H5N1 RNA in bronchial aspirate by RT-PCR. The durations of illness were 8, 10, 13, 16 and 18 days for cases 1, 2, 3, 4 and 5, respectively. The patients did not have significant medical histories or underlying diseases. All of them had a chance to be infected because of direct contact with sick poultry. Clinical symptoms exhibited by all patients included fever, cough and dyspnea. The average day of admission, which corresponded to when patients

complained of dyspnea, was day 8 of the illness. Soon after admission, they were placed on a ventilator because of reduced oxygen saturation. Laboratory data on admission showed that white blood cell count was low for all cases (1700–3400/mm^3). Antibiotics had been prescribed in all cases before admission. Antiviral treatment with oseltamivir was used in cases 2, 3 and 4 after admission. Methylpredonisolone was administered in all cases except for case 5. *Hemophilus influenza* was cultured from the sputa of case 5 on admission.

Histopathological Findings in the Lung

Acute intra-alveolar edema, congestion and/or hemorrhage, desquamation of pneumocytes, interstitial and intra-alveolar inflammatory cell infiltration, fibrosis and type II pneumocyte hyperplasia were observed. Three cases died before day 13 of the illness and presented with the exudative phase of diffuse alveolar damage (Figures 1a and c). The other two cases died after day 16 of the illness and presented with the proliferative phase of diffuse

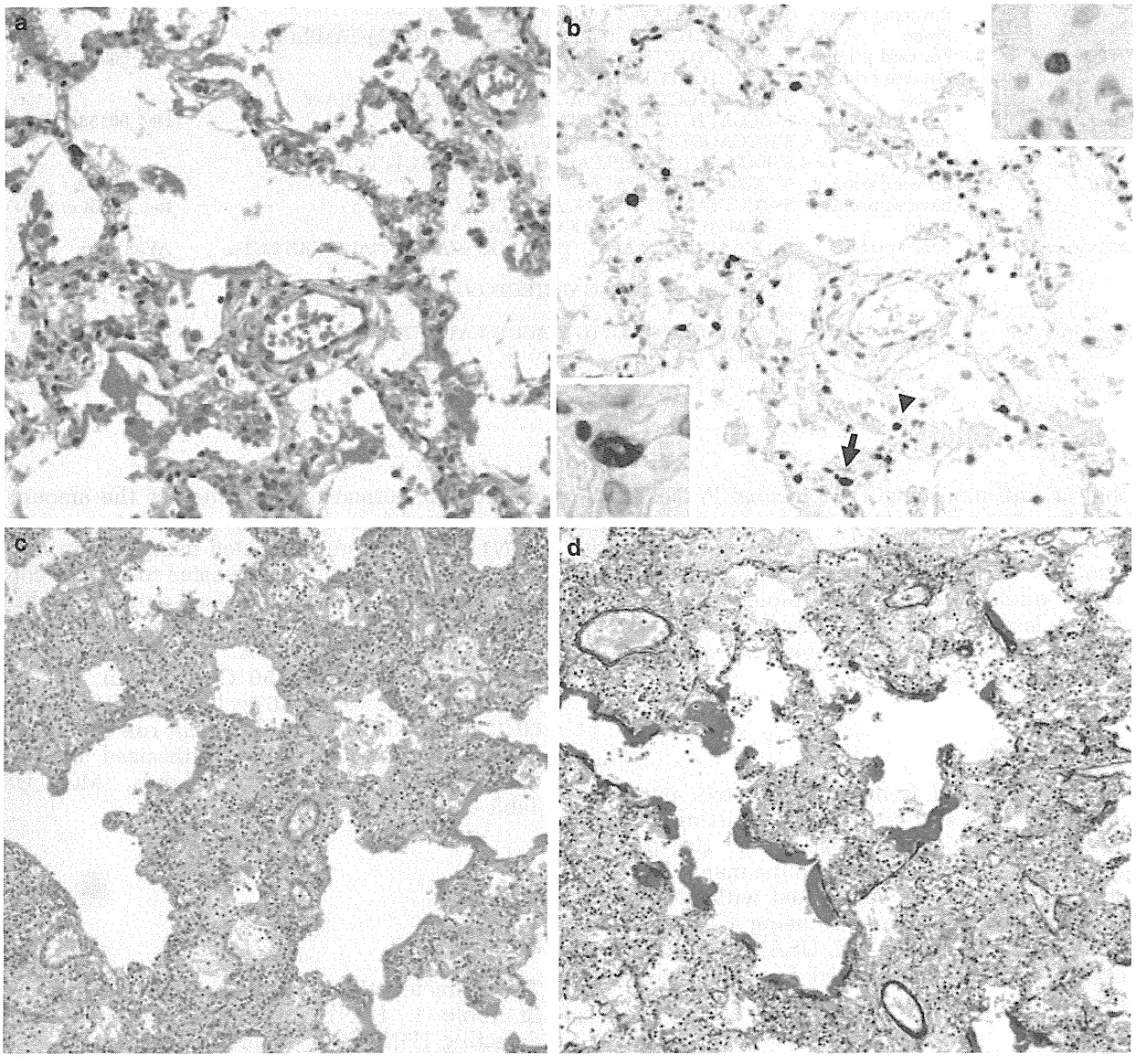

Figure 1 Representative histopathological findings in lung sections following hematoxylin–eosin (HE) (**a**, **c**, **e**) or Elastica–Masson Goldner staining (**d**). Immunohistochemistry was conducted to detect type A influenza virus nucleoprotein antigen (InfA-NP) (**b**). *In situ* hybridization AT-tailing (ISH-AT) (**f–h**) was also used. (**a**) Exudative phase of diffuse alveolar damage in Case 1. (**b**) InfA-NP antigen (brown) was detected in the nucleus (arrow head, upper inset) or cytoplasm (arrow, lower inset) of alveolar epithelial cells for Case 1. (**c**) Exudative phase of diffuse alveolar damage in case 3. (**d**) Elastica–Masson Goldner staining showed hyaline membrane formation (red) for case 3. (**e**) Proliferative phase of diffuse alveolar damage. The numbers of fibroblasts and myofibroblasts were increased in the alveolar septa and alveolar space in case 4. (**f**) ISH-AT using an antisense H5N1 nucleoprotein (NP) probe was able to detect H5N1 mRNA. (**g**) ISH-AT with a sense H5N1 NP probe detected H5N1 genomic RNA. (**h**) ISH-AT using an antisense rabies virus nucleocapsid probe as a negative control. Original magnifications, ×10 (**c**, **d**), ×20 (**a**, **b**), ×40 (**b**, inset, **f–h**).

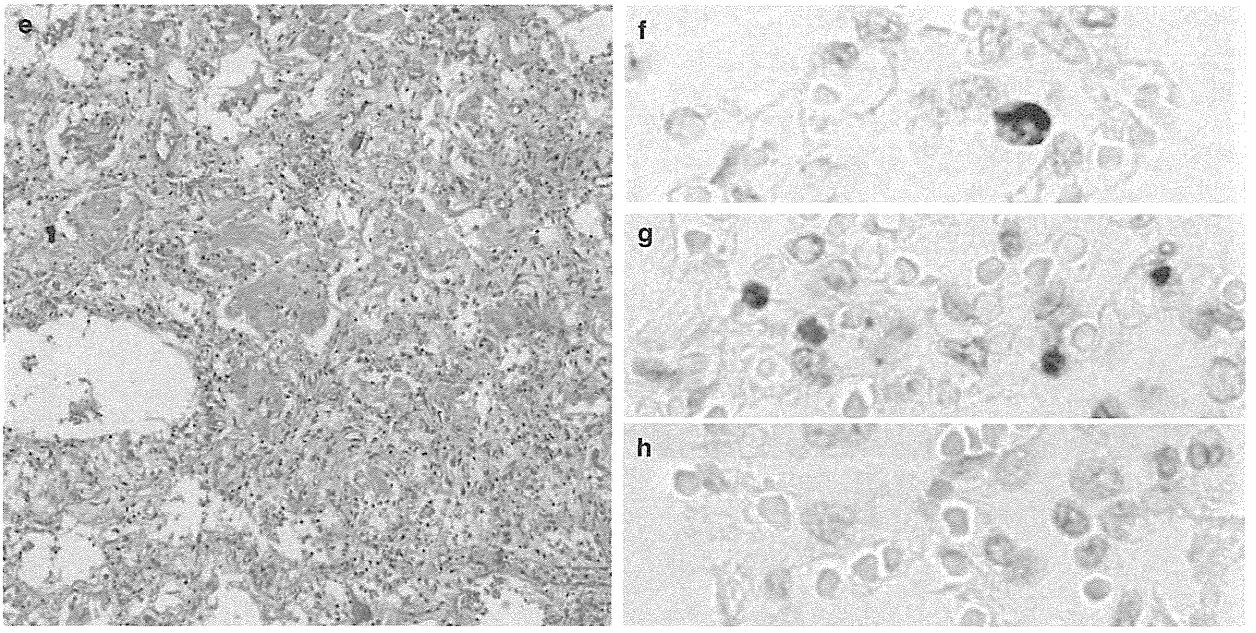

Figure 1 Continued.

alveolar damage. The numbers of myofibroblasts and fibroblasts were increased in case 4 (Figure 1e). Hyaline membrane formation was shown by Elastica–Masson Goldner staining (Figure 1d).

Histopathological Findings in Extrapulmonary Organs

Several extrapulmonary organs were examined in cases 2 and 3 (Table 1). Inflammatory cell infiltration was not observed in any sections from extrapulmonary tissues. In the liver, we observed focal mild fatty changes around a lobule with a ballooning change of hepatocytes in both cases. Reactive hemophagocytosis[3,5,6] and lymphoid depletion,[5,17] which are sometimes associated with hypercytokinemea, were not remarkable in the spleen. Renal tubular necrosis and congestion in the kidney[17] were not observed. The pathological findings in extrapulmonary organs from both cases were limited and appeared to be caused by hypoxic changes rather than H5N1 infection.

Characterization of Infiltrating Cells

The infiltrating cells in the alveolar septa and alveolar space (Figure 2a) were characterized using immunohistochemistry on serial lung sections from the exudative phase of diffuse alveolar damage. Most infiltrating cells were MPO-positive (Figure 2b) and/or CD68 clone KP-1-positive (Figure 2c). MPO was expressed in neutrophils, monocytes and their precursors. CD68 clone KP-1 was expressed in not only monocytes/macrophages but also myeloid precursors and neutrophils. Neutrophil elastase was expressed in some of the infiltrated cells, suggesting they were neutrophils or precursor cells (Figure 2d). CD68 clone PGM-1 is more specific for mature macrophages in comparison with CD68 clone KP-1. CD68 clone PGM-1-positive alveolar macrophages were also detected (Figure 2e). Taken together, the results indicate that the infiltrating cells were mainly neutrophils and monocytes/macrophages, and their precursors. CD8-positive cytotoxic T lymphocytes were rarely detected in this region (Figure 2f). Several CD8-positive T lymphocytes were detected in other areas of the same lung section, but there were few of these in total.

Viral Load

The relative levels of H5N1 viral RNA (genomic RNA and mRNA) in formalin-fixed, paraffin-embedded sections were quantified by qRT-PCR using primer-probe sets for the H5N1 M protein and β-actin gene sequences (Table 2). The relative H5N1 viral copy number per cell was calculated as described in the Materials and methods section. H5N1 RNA was under the detection limit (UDL) in all extrapulmonary tissue sections. The viral load varied among the lung regions from the same case (Figure 4a). The highest copy number of H5N1 RNA was seen from the lung in case 1, who had the shortest duration of illness. The lung in the proliferative phase of diffuse alveolar damage (cases 4 and 5) presented with a low viral load. In case 5, who died on day 18 of the disease, the amount of viral RNA was UDL in all lung sections (Figure 4a).

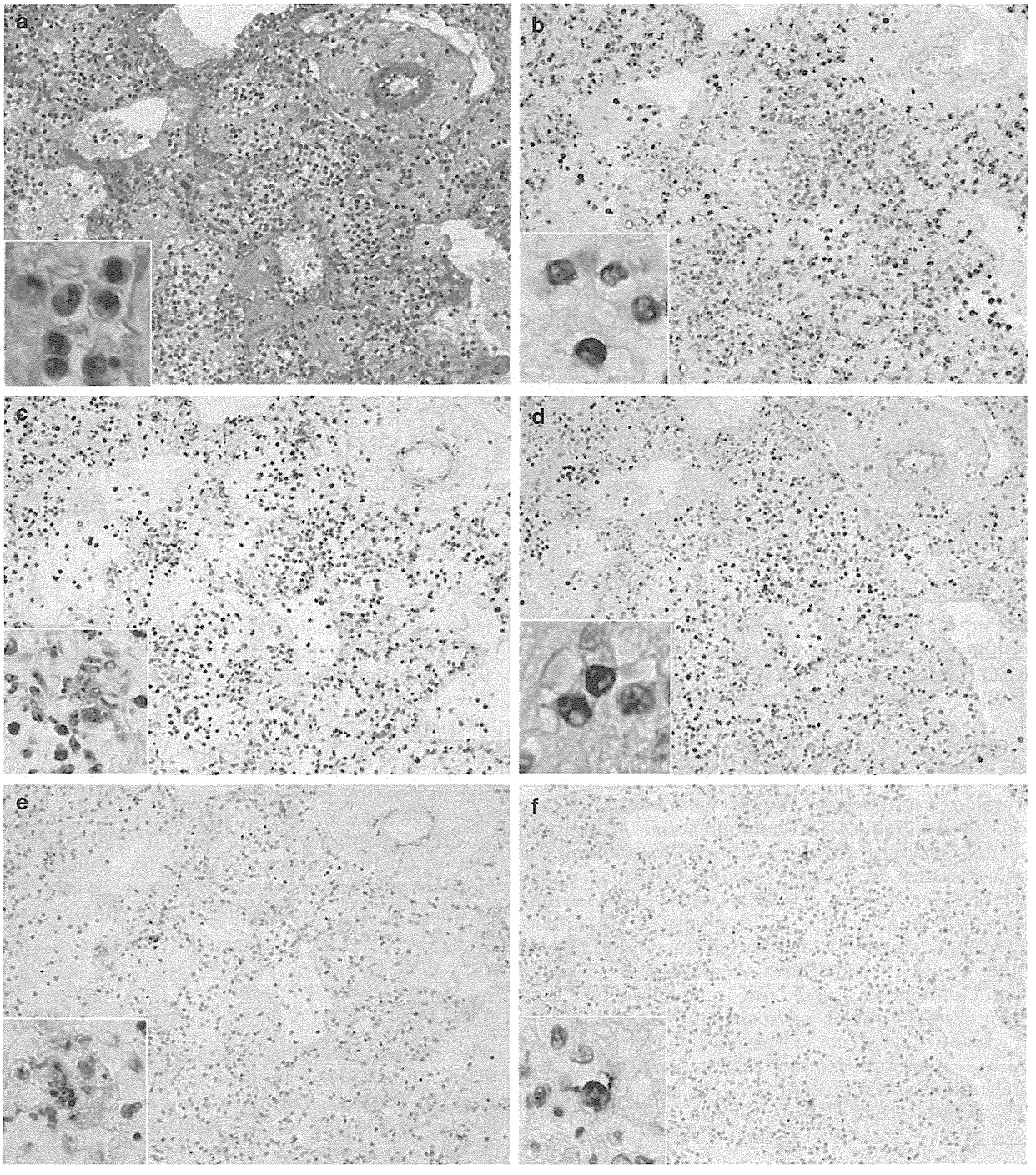

Figure 2 Hematoxylin–eosin (HE) staining (**a**) and immunohistochemistry for cell type-specific marker proteins (**b–f**) in serial lung sections from case 3. (**a**) Inflammatory cells infiltrated the alveolar septa and alveolar spaces. The phenotype of infiltrating cells were characterized using immunostaining for the detection of myeloperoxidase (MPO) (**b**), CD68 clone KP-1 (**c**), neutrophil elastase (**d**), CD68 clone PGM-1 (**e**) and CD8 T cells (**f**). Positive signals are indicated by brown staining. Original magnification, × 20 (**a–f**), × 40 (**a–f**, inset).

H5N1-Infected Cells Detected by Immunohistochemistry and *In Situ* Hybridization

The distribution of InfA-NP was examined by immunohistochemistry using monoclonal antibodies against the protein. It was detected in the lung tissue sections from cases 1, 2 and 3 (Table 1, Figure 1b). H5N1 mRNA and genomic RNA were detected separately in the lung sections of cases 1, 2 and 3 using ISH-AT with anti-sense and sense probes (Figures 1f and g). The detection of influenza mRNA was an indicator of virus proliferation in the

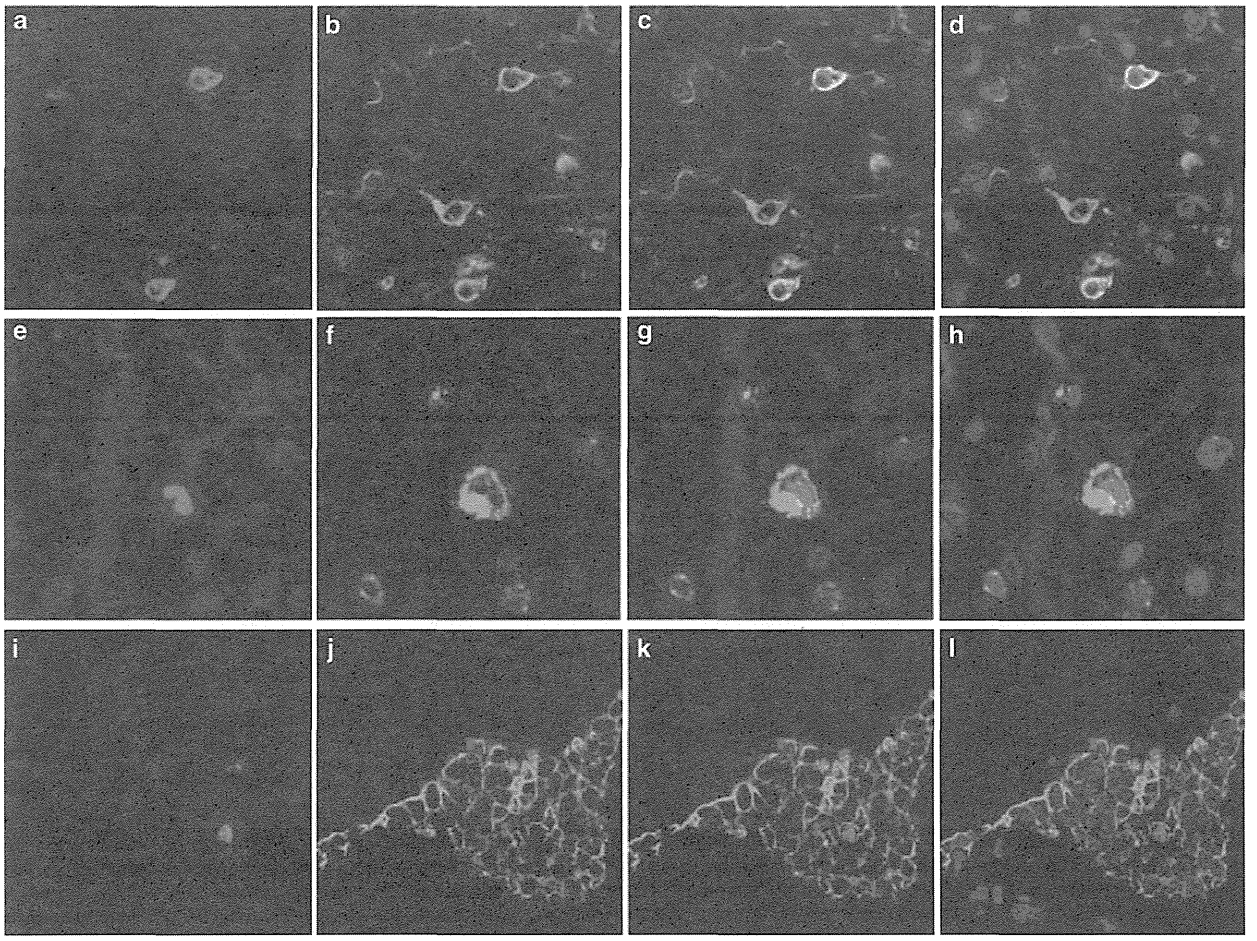

Figure 3 Phenotype of influenza A nucleoprotein antigen (InfA-NP)-positive cells. (**a**, **e**, **i**) InfA-NP immunoreactivity can be seen in red. (**b**) Immunoreactivity for surfactant apoprotein D (SP-D) in type II pneumocytes. (**f**) CD68 clone KP-1 in monocytes. (**j**) Cytokeratin (AE1/AE3) in bronchiolar epithelial cells. (**c**, **g**, **k**) Colocalization for each type is also presented. (**d**, **h**, **l**) TO-PRO-3 nucleic acid staining (blue) revealed the InfA-NP in nuclei. Original magnification, ×400.

lung. The InfA-NP-positive cells (red) were identified using double immunofluorescence staining for cell type-specific marker proteins (green) and TO-PRO-3 nucleic acid staining (blue). Positive signals were visualized by confocal laser scanning microscopy (Figure 3). The InfA-NP signals (Figures 3a, e and i) were mainly detected in the SP-D-positive type II pneumocytes (Figure 3b), and the CD68-positive monocytes/macrophages (Figure 3f). They were also detected in AE1/AE3-positive bronchiolar epithelial cells (Figure 3j). InfA-NP signals were detected in the nuclei (Figures 3d, h, and i).

Cytokines and Chemokines

The elevation of cytokine and chemokine levels occurred in H5N1-infected lungs. Their expression levels were examined by quantifying the mRNA copy number of TNF-α, IL-6, IL8, RANTES and IP-10 in the five cases. The extracted RNA from 3 to 5 lung regions from each case was analyzed separately. The expression levels were variable from every region of the same case. Case 1 presented with the highest titers of cytokines and chemokines of all. In case 5, only IL-8 mRNA was detected. The expression level of every cytokine and chemokine correlated with the copy number of H5N1 RNA (Figure 4g). This suggested that the local elevation of cytokines and chemokines in the lung were possibly caused by H5N1 infection in the same region.

Next, we tried to detect these cytokines and chemokines in the lungs of cases 1 and 3 using immunohistochemistry (Figure 5). TNF-α, IL-6, IL-8, RANTES and IP-10 were detected at much higher levels in case 1 compared with case 3, which was compatible with the copy number of each mRNA shown in Figure 4g. The phenotype of each cytokine/chemokine-positive cell was determined using double immunofluorescence staining. Cells expressing RANTES could not be identified. TNF-α was detected in a MPO-positive monocytes (Figure 6a-3) and SPD-positive type II pneumocytes (Figure 6b-3). IL-6 was detected in PGM-1-positive

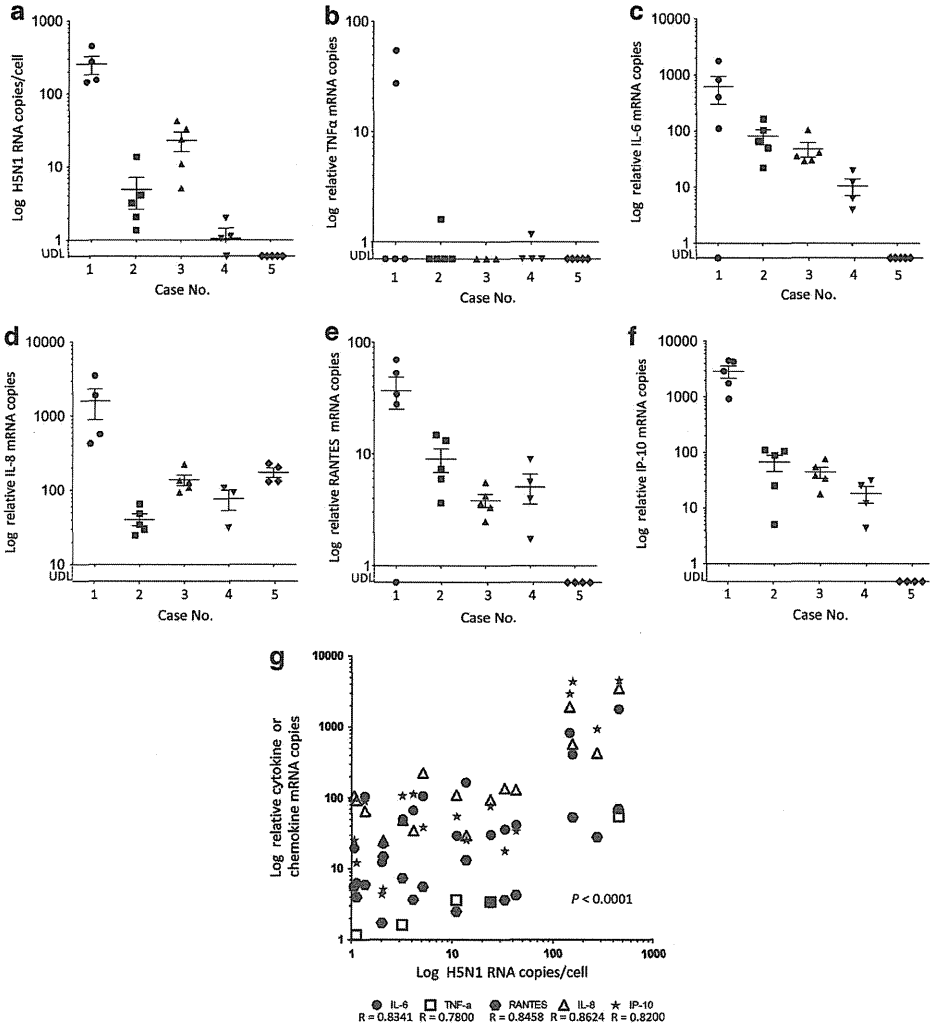

Figure 4 H5N1 RNA and proinflammatory cytokine or chemokine expression levels in several lung regions. The x axis indicates the case number. The durations of disease for cases 1, 2, 3, 4 and 5 were 8, 10, 13, 16 and 18 days, respectively. The y axis indicates H5N1 RNA (**a**), tumor necrosis factor-alpha (TNF-α) (**b**), interleukin (IL)-6 (**c**), IL-8 (**d**), regulated on activation normal T-cell expressed and secreted (RANTES) (**e**) and interferon-gamma-inducible protein of 10 kDa (IP-10) (**f**) mRNA copy numbers on a logarithmic scale. •, case 1; ■, case 2; ▲, case 3; ▼, case 4; and ◆, case 5. (**g**) Correlation between copy numbers of H5N1 RNA and cytokine or chemokine mRNA in lung tissue. Data from the five cases (**a–f**) were combined, with any values below the limit of detection (UDL) excluded. The horizontal lines indicate the mean, and vertical error bars indicate the mean ± s.d., $P<0.0001$.

monocytes/macrophages (Figure 6c-3) but also in an EMA-positive alveolar epithelial cells (Figure 6d-3) and in CD34-positive endothelial cells (Figure 6e-3). IL-8 was detected in PGM-1-positive monocytes/macrophages (Figure 6f-3). IP-10 was detected in PGM-1-positive monocytes/macrophages (Figure 6g-3) and EMA-positive bronchiolar epithelial cells (Figure 6h-3).

Discussion

All post-mortem biopsied or autopsied cases with H5N1 infection reported to date have shown acute respiratory distress syndrome clinically and diffuse alveolar damage in lung histopathology.[3–18] The five cases analyzed in this study also suffered from viral pneumonia, which led to acute respiratory distress syndrome. H5N1 antigens and RNA were detected in pneumocytes and monocytes/macrophages in cases 1, 2 and 3 (Figures 1e–g). In particular, these three cases presented with the exudative phase of diffuse alveolar damage *via* histopathology, with infiltration of inflammatory cells in the alveolar septa and alveolar space remarkably high. Immunohistochemistry revealed that the inflammatory cells were not lymphocytes, but mostly MPO- and/or CD68 clone KP-1-positive neutrophils or monocytes/macrophages (Figure 2). A more detailed study is necessary to elucidate the mechanism of infiltration for these cells in the H5N1-infected lung.

H5N1 patients presented with dysregulation of cytokine and chemokine levels, which is often referred to as a 'cytokine storm'. This is thought to

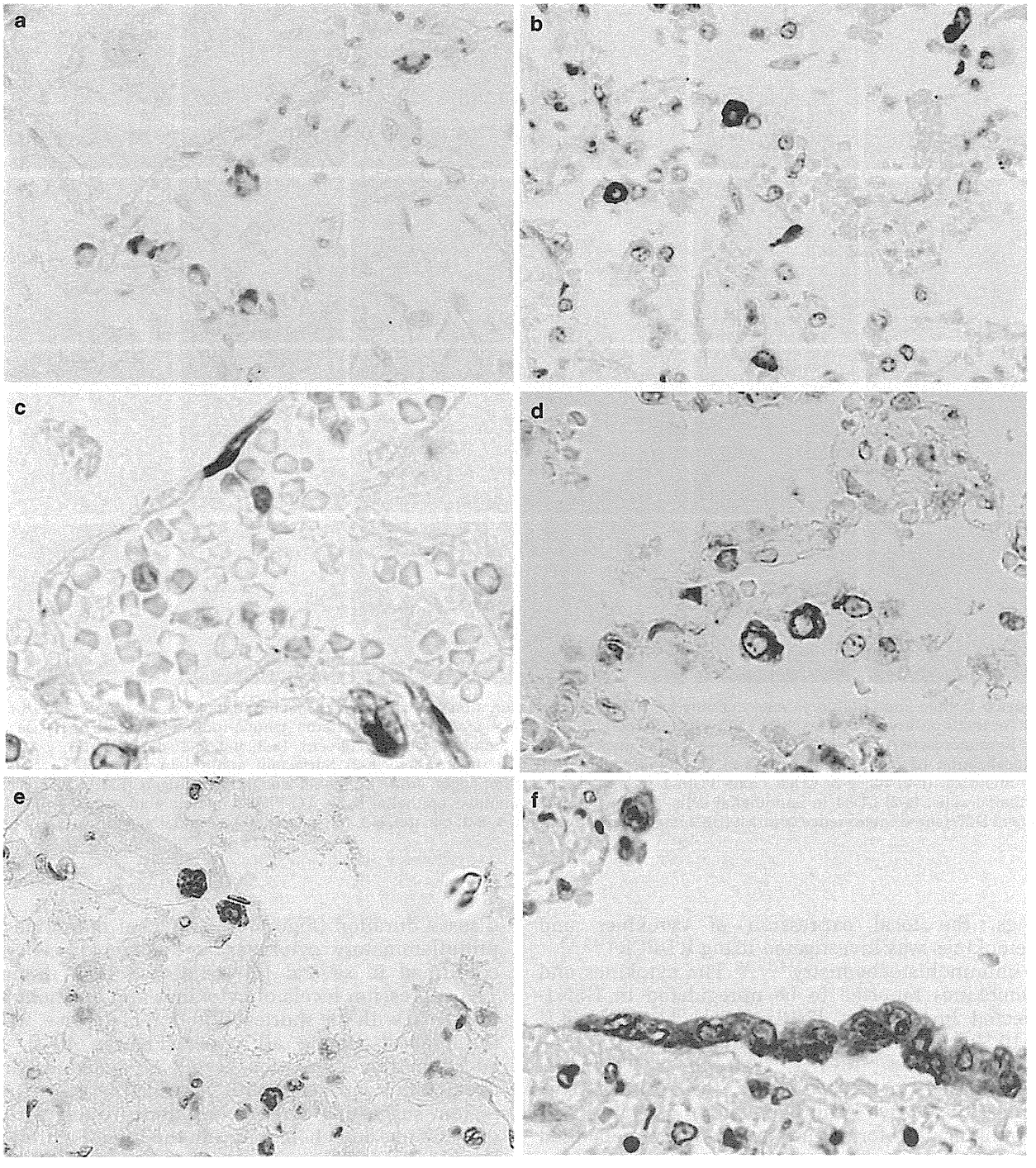

Figure 5 Immunohistochemistry on lung tissue sections for the detection of cytokines and chemokines. (**a**) Tumor necrosis factor-alpha (TNF-α), (**b**, **c**) interleukin (IL)-6, (**d**) IL-8, (**e**) regulated on activation normal T-cell expressed and secreted (RANTES) and (**f**) interferon-gamma-inducible protein of 10 kDa (IP-10) were detected in the cytoplasm of several cells. (**c**) IL-6 immunoreactivity was observed in endothelial cells. (**f**) IP-10 immunoreactivity was seen in bronchiolar epithelial cells. A positive signal is indicated by brown staining. Original magnification, $\times 40$.

be one of the key mechanisms in the pathogenesis of H5N1 infection.[3,33] According to *in vitro* experiments, H5N1 infection of primary human macrophages, along with alveolar and bronchial epithelial cells induced proinflammatory cytokines and chemokines more potently than seasonal influenza virus infection.[34–36] Animal experiments also showed induction of proinflammatory cytokines and chemokines occurred because of H5N1 infection.[37,38] In H5N1-infected human

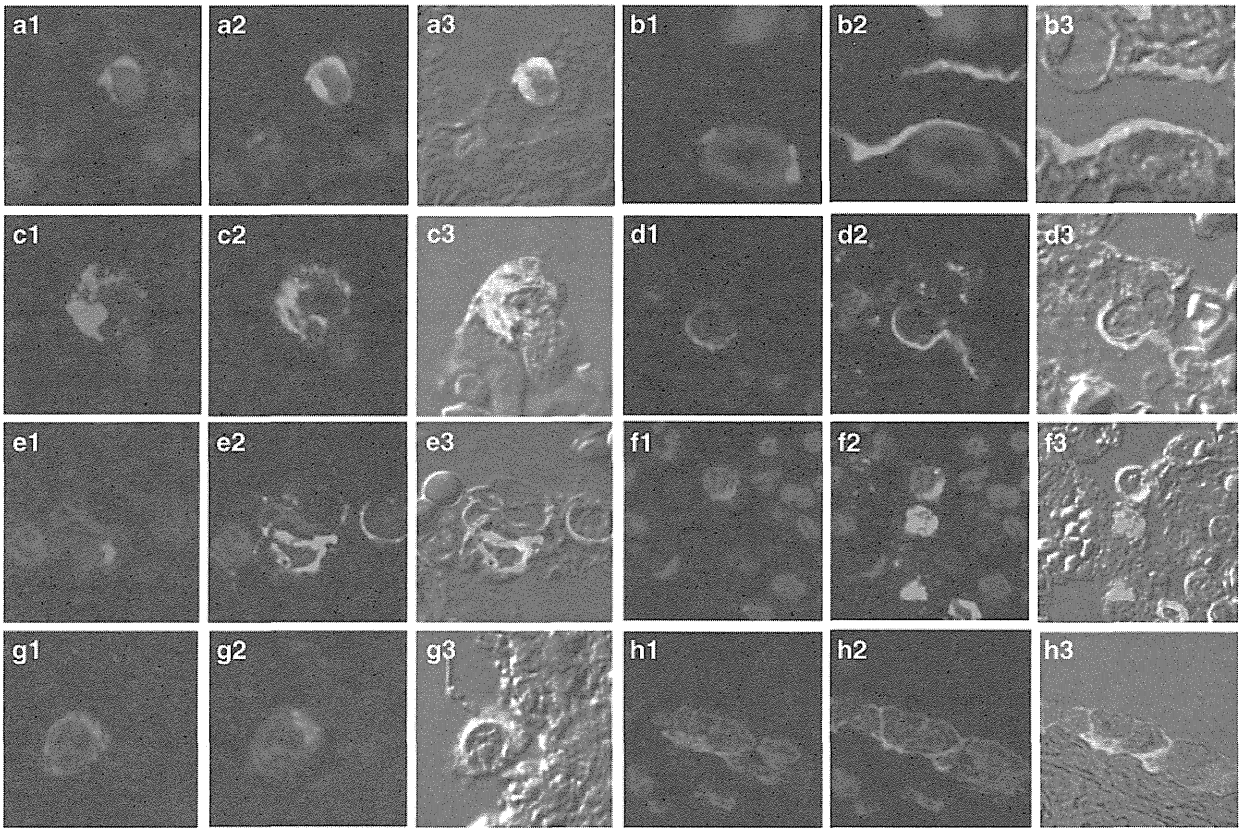

Figure 6 Double immunofluorescence staining for phenotype determination of tumor necrosis factor-alpha (TNF-α), interleukin (IL)-6-, IL-8- or IP-10-positive cells. (**a-1**, **b-1**) TNF-α, (**c-1**, **d-1**, **e-1**) IL-6, (**f-1**) IL-8 and (**g-1**, **h-1**) interferon-gamma-inducible protein of 10 kDa (IP-10) immunoreactivity (red) and cell type-specific marker protein immunoreactivity (green). (**a-3**, **b-3**, **c-3**, **d-3**, **e-3**, **f-3**, **g-3**, **h-3**) Colocalization of immunostaining. (**a-2**) Myeloperoxidase (MPO) in monocytes. (**b-2**) Surfactant apoprotein D (SP-D) in type II pneumocytes. (**c-2**, **f-2**, **g-2**) CD68 clone PGM-1 in monocytes/macrophages. (**d-2**) Epithelial membrane antigen (EMA) in alveolar epithelial cells. (**e-2**) CD34 in endothelial cells. (**h-2**) EMA in bronchiolar epithelial cells. TO-PRO-3 nucleic acid staining (blue) is shown. Differential interference contrast (DIC) images are shown in **a-3**, **b-3**, **c-3**, **d-3**, **e-3**, **f-3**, **g-3** and **h-3**. Original magnification, × 600.

lungs, the local expression of cytokines and chemokines was investigated using RT-PCR[9–11,13,17] or immunohistochemistry.[4,15,16] The cytokines and chemokines reported to be upregulated in H5N1-infected lungs were: TNF-α,[4,9,10,13,16,17] IFN-α/β,[11] IP-10,[11,13,16,17] RANTES,[16,17] MIP-3β,[17] IL-6,[16] IFN-γ,[16] IFN-β,[16] IL-8,[16] MCP-1,[16] and MIP-1α.[15,16] In this study, based on these findings, we quantified the expression of five proinflammatory cytokines and chemokines in formalin-fixed, paraffin-embedded H5N1-infected lung tissues. We examined 3–5 lung regions per case. It was impossible to examine the time course of expression for each mediator in the post-mortem biopsied or autopsied lungs. The five patients in this study had no significant medical histories or underlying diseases, which could possibly affect expression levels of cytokines and chemokines. Furthermore, all formalin-fixed, paraffin-embedded samples were prepared using the same procedures at the same hospital. We have presented the expression levels of each mediator in the lungs of the five cases in order of shortness of disease duration (Figure 4). The local induction of proinflammatory cytokines and chemokines were confirmed in several H5N1-infected lung tissues. The expression levels of cytokines and chemokines in case 1, with the shortest duration of disease, were the highest among all cases (Figures 4b–f). In addition, the expression levels of cytokines and chemokines correlated with viral load in every lung region, suggesting that H5N1-induced upregulation of cytokines and chemokines in the lung (Figure 4g). Double immunofluorescence staining revealed that cells expressing the cytokines and chemokines were mainly monocytes/macrophages or epithelial cells (Figure 6). Our results were consistent with those previously reported.[4,16] We also noticed the new finding that IL-6 was expressed in EMA-positive alveolar epithelial cells (Figure 6d-3), CD34-positive endothelial cells (Figure 6e-3), and PGM-1-positive monocytes/macrophages (Figure 6c-3). It should be noted that IL-6 was also detected in endothelial cells, which may be related to local vascular injury in H5N1-infected lung (Figure 6e-3).

The most important characteristics of H5N1 infection that distinguish it from other subtypes of influenza virus infection, are that H5N1 disseminates beyond the respiratory system.[14] For disseminated infection, H5N1 should have been in the bloodstream at some point. Virus isolation from peripheral blood is considered evidence of viremia.[33,39] Actually, virus antigens and H5N1 RNA have been reported to be detected in extrapulmonary tissues from several fatal cases.[6,9,10,12–15,17] The positive strand of H5N1 mRNA, indicative of viral replication, was detected by strand-specific RT-PCR in the intestines,[6,13,14] liver,[9,13] heart,[13,14] lymph node,[13] placenta[14] and brain.[14] On the other hand, histopathological findings were mostly nonspecific for H5N1 infection, such as hemophagocytotic activity, depletion of lymphoid cells, acute tubular necrosis, fatty changes in the liver and brain edema. More specific pathological changes, such as inflammatory cell infiltrations associated with the detection of viral antigen would be needed to show disseminate H5N1 infection. In extrapulmonary organs of two autopsied cases in this study, we were unable to obtain evidence of H5N1 dissemination. For both cases, illness lasted >10 days and the titers of H5N1 RNA were low, even in lung sections (Table 1, Figure 4a). Therefore, it might be reasonable to suggest that H5N1 RNA in extrapulmonary organs were below the level of detection. In addition, the histopathological findings of the extrapulmonary tissues were limited to nonspecific ischemic changes. The inconsistent results regarding the extent of H5N1 distribution in fatal cases are likely due to several factors, including the conditions of samples, the duration of disease and the medication given to patients. In addition to this, the differences in permissivity and immunological reactivity to H5N1 among patients should be also considered.

We investigated formalin-fixed, paraffin-embedded tissues from five fatal H5N1 cases. H5N1 viral load was highest in the lung of the case with the shortest duration of disease. Proinflammatory cytokine and chemokine mRNA copy numbers correlated with H5N1 RNA copy numbers in each lung region. In H5N1-infected lungs, monocytes/macrophages, epithelial cells and endothelial cells produced several cytokines and chemokines. We were unable to determine any dissemination of H5N1 beyond the respiratory organs in two autopsied cases. Further investigation is necessary to elucidate the pathogenesis of H5N1 infection in humans.

Acknowledgements

We thank Dr Thuy TB Phung for clinical information of patients and Ms K Shimonohara for technical assistance. This work was supported by the Health and Labor Sciences Research Grants on Emerging and Re-emerging Infectious Diseases (H22 Shinko-Ippan-014), from the Ministry of Health, Labour and Welfare, Japan.

Disclosure/conflict of interest

The authors declare no conflict of interest.

References

1 Beigel JH, Farrar J, Han AM, *et al.* Avian influenza A (H5N1) infection in humans. N Engl J Med 2005;353:1374–1385.
2 Yuen KY, Chan PK, Peiris M, *et al.* Clinical features and rapid viral diagnosis of human disease associated with avian influenza A H5N1 virus. Lancet 1998;351: 467–471.
3 To KF, Chan PKS, Chan KF, *et al.* Pathology of fatal human infection associated with avian influenza A H5N1 virus. J Med Virol 2001;63:242–246.
4 Peiris JSM, Yu WC, Leung CW, *et al.* Re-emergence of fatal human influenza A subtype H5N1 disease. Lancet 2004;363:617–619.
5 Ng WF, To KF, Lam WWL, *et al.* The comparative pathology of severe acute respiratory syndrome and avian influenza A subtype H5N1-a review. Hum Pathol 2006;37:381–390.
6 Zhang Z, Zhang J, Huang K, *et al.* Systemic infection of avian influenza A virus H5N1 subtype in human. Hum Pathol 2009;40:735–739.
7 Ungchusak K, Aucwarakul P, Dowell SF, *et al.* Probable person-to-person transmission of avian influenza (H5N1). N Engl J Med 2005;352:333–340.
8 Chotpitayasunondh T, Ungchusak K, Hanshaoworakul W, *et al.* Human disease from influenza A (H5N1), Thailand, 2004. Emerg Infect Dis 2005;11:201–209.
9 Uiprasertkul M, Puthavathana P, Sangsiriwut K, *et al.* Influenza A H5N1 replication sites in humans. Emerg Infect Dis 2005;11:1036–1041.
10 Uiprasertkul M, Kitphati R, Puthavathana P, *et al.* Apoptosis and pathogenesis of avian influenza A (H5N1) virus in Humans. Emerg Infect Dis 2007;13:708–712.
11 Thitithanyanont A, Engering A, Uiprasertkul M, *et al.* Antiviral immune response in H5N1-infected human lung tissue and possible mechanisms underlying the hyper production of interferon-inducible IP-10. Biochem Biophys Res Commun 2010;398:752–758.
12 Piwpankaew Y, Monteerarat Y, Suptawiwat O, *et al.* Distribution of viral RNA, sialic acid receptor, and pathology in H5N1 avian influenza patients. Acta Pathol Microbiol Scand 2010;118:895–902.
13 Sirinonthanawech N, Uiprasertkul M, Suptawiwat O, *et al.* Viral load of the highly pathogenic avian influenza H5N1 virus in infected human tissues. J Med Virol 2011;83:1418–1423.
14 Gu J, Xie Z, Gao Z, *et al.* H5N1 infection of the respiratory tract and beyond: a molecular pathology study. Lancet 2007;370:1137–1145.
15 Korteweg C, Gu J. Pathology, molecular biology, and pathogenesis of avian influenza A (H5N1) infection in humans. Am J Pathol 2008;172:1155–1170.

16 Deng R, Lu M, Korteweg C, *et al.* Distinctly different expression of cytokines and chemokines in the lung of two H5N1 avian influenza patients. J Pathol 2008;216:328–336.
17 Gao R, Dong L, Dong J, *et al.* A systemic molecular pathology study of a laboratory confirmed H5N1 human case. PLoS ONE 2010;5:e13315.
18 Liem NT, Nakajima N, Phat LP, *et al.* H5N1-infected cells in lung with diffuse alveolar damage in exudative phase from a fatal case in Vietnam. Jpn J Infect Dis 2008;61:157–160.
19 Taubenberger JK, Morens DM. The pathology of influenza virus infections. Annu Rev Pathol 2008;3:499–522.
20 Guarner J, Shieh WJ, Dawson J, *et al.* Immunohistochemical and in situ hybridization studies of influenza A virus infection in human lungs. Am J Clin Pathol 2000;114:227–233.
21 Guarner J, Pddock CD, Shieh WJ, *et al.* Histopathologic and immunohistochemical features of fatal influenza virus infection in children during the 2003–2004 season. Clin Infect Dis 2006;43:132–140.
22 Soto-Abraham MV, Soriano-Rosas J, Diaz-Quinonez A, *et al.* Pathological changes associated with 2009 H1N1 virus. N Engl J Med 2009;361:2001–2003.
23 Nakajima N, Hata S, Sato Y, *et al.* The first case of pandemic influenza (A/H1N1) virus infection in Japan: Detection of a high copy number of the virus in type II alveolar epithelial cells by pathological and virological examination. Jpn J Infect Dis 2010;63:67–71.
24 Maud T, Hajjar LA, Callegari GD, *et al.* Lung pathology in fatal novel human influenza A (H1N1) infection. Am J Respir Crit Care Med 2010;181:72–79.
25 Gill JR, Sheng ZM, Ely SF, *et al.* Pulmonary pathologic findings of fatal 2009 pandemic influenza A/H1N1 viral infections. Arch Pathol Lab Med 2010;134: 235–243.
26 Shieh WJ, Blau DM, Denison AM, *et al.* 2009 Pandemic influenza A (H1N1): pathology and pathogenesis of 100 fatal cases in the United States. Am J Pathol 2010;177:166–175.
27 Nakajima N, Sato Y, Katano H, *et al.* Histopathological and immunohistochemical findings of 20 autopsy cases with 2009 H1N1 virus infection. Modern Pathol 2012;25:1–13.
28 Chen Z, Sahashi Y, Matsuo K, *et al.* Comparison of the ability of viral protein- expressing plasmid DNAs to protect against influenza. Vaccine 1998;16:1544–1549.
29 Nakajima N, Petronela Ionescu, Sato Y, *et al.* In situ hybridization AT-tailing with catalyzed signal amplification for sensitive and specific in situ detection of human immunodeficiency virus -1 mRNA in formaline-fixed and paraffin-embedded tissues. Am J Pathol 2003;2:381–389.
30 Nakajima N, Ozaki YA, Nagata N, *et al.* SARS Coronavirus-infected cells in lung detected by new in situ hybridization technique. Jpn J Infect Dis 2003;56:139–141.
31 Ng EK, Cheng PK, Ng AY, *et al.* Influenza A H5N1 detection. Emerg Infect Dis 2005;11:21303–21305.
32 Krafft AE, Russell KL, Hawksworth AW, *et al.* Evaluation of PCR testing of ethanol-fixed nasal swab specimens as an augumented surveillance strategy for influenza virus and adenovirus identification. J Clin Microbiol 2005;43:1768–1775.
33 De Jong MD, Simmons CP, Thanh TT, *et al.* Fatal outcome of human influenza A (H5N1) is associated with high viral load and hypercytokinemia. Nat Med 2006;12:1203–1207.
34 Cheung CY, Poon LLM, Lau AS, *et al.* Induction of proinflammatory cytokines in human macrophages by influenza A (H5N1) viruses: a mechanism for the unusual severity of human disease? Lancet 2002;360:1831–1837.
35 Chan MC, Cheung CY, Chui WH, *et al.* Proinflammatory cytokine reponses induced by influenza A (H5N1) viruses in primary human alveolar and bronchial epithelial cells. Respir Res 2005;6:135.
36 Lam WY, Yeung AC, Chu IM, *et al.* Profiles of cytokine and chemokine gene expression in human pulmonary epithelial cells induced by human and avian influenza viruses. Virol J 2010;7:344.
37 Baskin CR, Bielefeldt-Ohmann H, Tumpey TM, *et al.* Early and sustained innate immune response defines pathology and death in nonhuman primates infected by highly pathogenic influenza virus. Proc Natl Acad Sci USA 2009;9:3455–3460.
38 Maines TR, Belser JA, Gustin KM, *et al.* Local innate immune responses and influenza virus transmission and virulence in ferrets. J Infect Dis 2012;205:474–485.
39 Chutinimithul S, Bhattarakosol P, Srisuratanon S, *et al.* H5N1 influenza A virus and infected human plasma. Emerg Infect Dis 2006;12:1041–1043.

Microbiology and Immunology

Microbiol Immunol 2012; **56**: 171–182
doi:10.1111/j.1348-0421.2011.00424.x

ORIGINAL ARTICLE

Contribution of neutrophil-derived myeloperoxidase in the early phase of fulminant acute respiratory distress syndrome induced by influenza virus infection

Ryuichi Sugamata[1,2], Hideki Dobashi[1,2], Tomokazu Nagao[1,2], Ki-ichi Yamamoto[2], Noriko Nakajima[3], Yuko Sato[3], Yasuaki Aratani[4], Masamichi Oshima[2], Tetsutaro Sata[3], Kazuo Kobayashi[2], Shoji Kawachi[5], Toshinori Nakayama[6] and Kazuo Suzuki[1,2]

[1]Inflammation Program, [6]Department of Immunology, Graduate School of Medicine, Chiba University, Inohana 1-8-1, Chuo-ku, Chiba-city, Chiba 260-8670, Departments of [2]Immunology and [3]Pathology, National Institute of Infectious Diseases, Toyama 1-23-1, Shinjuku-ku, Tokyo 162-8640, [4]Graduate School of Nanobioscience, Yokohama City University, Seto 22-2, Kanazawa-ku, Yokohama-city, Kanagawa 236-0027, and [5]Division of Anesthesia, Surgical Operation Department, National Center for Global Health and Medicine, Toyama 1-21-1, Shinjuku-ku, Tokyo 162-8655, Japan

ABSTRACT

Because the pathogenesis of acute respiratory distress syndrome (ARDS) induced by influenza virus infection remains unknown, we can only improve on existing therapeutic interventions. To approach the subject, we investigated immunological etiology focused on cytokines and an acute lung damage factor in influenza-induced ARDS by using a PR-8 (A/H1N1)-infected mouse model. The infected mouse showed fulminant severe pneumonia with leukocyte infiltration, claudin alteration on tight junctions, and formation of hyaline membranes. In addition to interferon (IFN)-α, plenty of keratinocyte-derived chemokines (KC), macrophage inflammatory protein 2 (MIP-2), regulated on activation normal T-cell expressed and secreted (RANTES), and monocyte chemotactic protein 1 (MCP-1) were significantly released into bronchoalveolar lavage fluid (BALF) of the model. We focused on neutrophil myeloperoxidase (MPO) as a potent tissue damage factor and examined its contribution in influenza pneumonia by using mice genetically lacking in MPO. The absence of MPO reduced inflammatory damage with suppression of leakage of total BALF proteins associated with alteration of claudins in the lung. $MPO^{-/-}$ mice also suppressed viral load in the lung. The present study suggests that MPO-mediated OCl^- generation affects claudin molecules and leads to protein leakage and viral spread as a damage factor in influenza-induced ARDS.

Key words acute respiratory distress syndrome (ARDS), influenza, myeloperoxidase (MPO), neutrophil.

Acute respiratory distress syndrome is provoked by ALI with pulmonary edema, capillary leak, and hypoxemia, which is a severe clinical state triggered by both infectious and non-infectious stimuli (1). The Spanish influenza (A/H1N1) pandemic of 1918 and pandemic influenza (A/H1N1pdm) have been shown to cause ARDS under specific conditions in humans (2,3). The current emergence of highly pathogenic avian influenza virus (A/H5N1) has been documented to cause fulminant ARDS (called FARDS), which is characterized by more rapid progression of pathology with short duration (4,5). ARDS caused by these influenza virus infections brings on

Correspondence
Kazuo Suzuki, Inflammation Program, Department of Immunology, Graduate School of Medicine, Chiba University, Inohana 1-8-1, Chuo-ku, Chiba-city, Chiba 260-8670, Japan.
Tel: +81 43 221 0831; fax: + 81 43 221 0832; email: ksuzuki@faculty.chiba-u.jp

Received 4 August 2011; revised 21 December 2011; accepted 22 December 2011.

Abbreviations: ALI, acute lung injury; ARDS, acute respiratory distress syndrome; BALF, bronchoalveolar lavage fluid; dpi, days post-infection; G-CSF, granulocyte-colony stimulating factor; GM-CSF, granulocyte/macrophage colony-stimulating factor; IFN, interferon; IL, interleukin; IRF, interferon regulatory factor; KC, keratinocyte-derived chemokine; MCP-1, monocyte chemotactic protein 1; MIP-2, macrophage inflammatory protein 2; MPO, myeloperoxidase; RANTES, regulated on activation normal T-cell expressed and secreted; TJ, tight junction; TNF, tumor necrosis factor.

a great deal of lethality. However, the precise pathogenesis of fulminant pneumonia associated with influenza virus infection remains unknown and thus it is difficult to develop appropriate therapeutic interventions.

Influenza virus-induced ARDS is pathologically shown by diffuse alveolar damage with fibrinous exudates, edema, and hyaline membranes in a category of ALI (3–6). Lung injury is associated with altered expression of claudin molecules in lung TJ (7,8). In addition, some inflammatory cytokines produced during lung inflammation alter composition of claudin in TJ (7–9). This change in claudin collapses barrier functions and leads to pulmonary edema resulting in the lung injury (8). However, claudin alteration in the early phase of lung tissue damage triggered by influenza virus infection has never been fully investigated. Therefore, the study of claudin alteration at lung TJ in influenza pneumonia would provide useful information on claudin function.

Influenza virus infection induces leukocyte infiltration into pulmonary alveoli. The majority of infiltrating leukocytes consist of neutrophils and macrophages (10), which are recruited by specific chemokines such as MIP-2 (CXCL2) and MCP-1 (CCL2) produced from lung tissue by infection (11). Neutrophils, which infiltrate in the earliest phase of infection, degrade and inactivate viral proteins with ROS production mediated by MPO abundantly contained in azurophil granules (12,13). The depletion of neutrophils leads to lethal viremia in experimental models, indicating that neutrophils contribute to clearance of influenza virus (10). However, the relation of a massive influx of neutrophils to aggravation of lung damage has been noted (12,14–16). The spectrum of neutrophil activity reflects both the killing of pathogens and tissue damage. In influenza pneumonia, it is possible that neutrophil MPO is associated with aggravation of inflammatory damage in the lung as well as degradation of viral proteins (14). The pathogenic roles of MPO in influenza pneumonia remain to be clarified.

In the present study, we established an animal model of fulminant ARDS induced by influenza virus infection. We characterized the dominant chemokines for leukocyte infiltration in lung tissue during the early phase of severe influenza pneumonia. We further investigated the association of neutrophil MPO with inflammatory damage induced by influenza virus infection, focusing on cytokines, claudin alteration, and viral load using $MPO^{-/-}$ mice.

MATERIALS AND METHODS

Mice

Animal protocols were approved by the Institutional Animal Use and Care Committee and conformed to the guidelines of the National Institute of Infectious Diseases (NIID). Wild-type female 8-week-old BALB/c mice were purchased from SLC (Shizuoka, Japan). Same-age female mice (BALB/c) genetically lacking in MPO were also prepared (17,18). Mice were housed in pathogen-free conditions to prevent secondary pathogenic infection according to the guidelines of the NIID.

Viral infection, harvesting, and histopathology

A mouse-adapted strain of influenza virus, A/Puerto Rico/8/34 (A/PR/8/34; PR-8), was supplied by the NIID. The virus strain was propagated in embryonated hen's eggs and stored at −80°C until use. Each mouse was lightly anesthetized with an intraperitoneal (i.p.) injection of pentobarbital sodium and was infected intranasally with 1400 plaque-forming units (p.f.u.) of PR-8 in 30 μL RPMI-1640 medium supplemented with 2% FBS. Control mice were mock-infected with the supplemented medium only. At each indicated dpi, mice were killed by terminal anesthesia, and lavage fluid was harvested via trachea by three lavages, each with 1 mL physiological saline solution. The lavage fluid was pooled and spun at 430 × g for 5 min to pellet bronchoalveolar lavage (BAL) cells. BALF supernatant was saved for Multi-plex and ELISA as described below. The BAL cells were used for cytospin preparation.

After BALF collection, the left lung lobe was removed and fixed with 10% formalin neutral buffer solution (Wako, Osaka, Japan) for at least 72 hrs. The fixed tissues were embedded in paraffin and cut into 5-μm-thick sections for hematoxylin and eosin (HE) stains and into 3-μm sections for Masson's trichrome stains and immunohistochemistry (IHC), respectively. The right lung lobe was collected and immediately fixed by RNAlater (Takara Bio, Shiga, Japan). Total RNA was extracted from the fixed lung tissues using TRIzol reagent (Invitrogen, Carlsbad, CA, USA) in accordance with the manufacturer's instructions.

Measurement of cytokine proteins

Interferon-alpha protein in the BALF was quantitated by an ELISA Kit (PBL InterferonSource, Piscataway, NJ, USA) according to the manufacturer's instructions. Other cytokine and chemokine proteins in the BALF and plasma were measured by Multi-plex analysis using Luminex (Millipore, Billerica, MA, USA) on the Bio-plex reader (Bio-Rad, Hercules, CA, USA).

Measurement of MPO activity

Myeloperoxidase activity in the BALF was measured by the TMB (3,3′,5,5′ tetramethylbenzidine) method (19). After

the plate was incubated with a substrate buffer containing TMB solution, an increase in absorbance at 650 nm for 5 min was measured by the Bio-Rad automatic reader system (Model 680-microplate reader; Bio-Rad). The activity was calculated as units/min per mL.

Quantitative real-time PCR and RT-PCR analyses

Total RNA extracted from the right lung specimen was treated with DNase (TURBO DNA-*free*; Ambion, Austin, TX, USA) and used as a template to synthesize cDNA with the Superscript VILO cDNA Synthesis Kit (Invitrogen). Using specific primer sets (Table S1), the expression of each gene was quantitated with SYBR Green PCR Master Mix (Applied Biosystems, Foster City, CA, USA) by the StepOne Real-Time PCR System (Applied Biosystems). Reaction conditions were 95°C for 15 s and 60°C for 1 min, repeated for 40 cycles, with hot start at 95°C for 10 min. Each PCR analysis was run in duplicate for each sample, and the expression level of each cytokine was normalized by the expression of either β-actin or glyceraldehyde-3-phosphate dehydrogenase (GAPDH).

Immunohistochemistry

Sections (3-μm thick) were mounted on silicone-coated glass slides. After deparaffinization, the sections were treated with 0.025% trypsin at 37°C for 30 min and washed with PBS. After incubation in blocking solution for 20 min at room temperature, the sections were reacted with rabbit anti-influenza type A nucleoprotein (InfA-NP) polyclonal antibody (6) at 4°C overnight. After being washed three times with TBS, the sections were stained by the avidin-biotin complex immunoperoxidase method (LSAB kit/HRP/DAB; DAKO Cytomation, Copenhagen, Denmark). Signals were detected by the CSA method using a CSA-II kit (DAKO).

Assessment of lung damage by neutrophil functions

$MPO^{-/-}$ and wild-type mice were infected intranasally with 1400 p.f.u. PR-8 in 30 μL RPMI-1640 medium supplemented with 2% FBS. As described above, infected mice were killed, BALF was collected, and the left and right lung lobes were removed separately. MPO activity in BALF was measured by the TMB oxidation method, as previously reported (19). Concentration of total protein in BALF was determined with a DC assay kit (Bio-Rad), and cytokines/chemokines produced in the BALF were quantitated by the Multi-plex analysis. To compare the histology between $MPO^{-/-}$ and wild-type mice, HE stains and immunohistochemistry (IHC) were applied to the left lung lobe. Total RNA was extracted from the right lung lobe, and cDNA was synthesized by the method mentioned above. The cDNA was subjected to quantitative expression of virus and claudin gene expression by quantitative real-time PCR.

Statistical analysis

The number of mice used in each experiment is shown in the respective figure legend. Statistical analyses of claudin profile, cytokine levels, and viral gene expression were carried out using Student's *t*-test for paired variables. Data are expressed as the mean ± standard deviation about the mean. Asterisks denote statistically significant results relative to those in uninfected mice: $^{*}P < 0.05$, $^{**}P < 0.01$, and $^{***}P < 0.001$.

RESULTS

Histopathology of the lung induced by influenza virus infection

To establish a mouse model for ARDS induced by influenza virus infection, BALB/c mice were challenged with a high dose of PR-8 virus, 1400 p.f.u. Inflammation was observed at the bronchiolar and alveolar epithelium. On 3 dpi, edema in the interstitial spaces and alveolar wall disruption were observed, and these became severe on 4 dpi (Fig. 1a). Inflammatory cells were found to have infiltrated around the bronchus and alveolus, and they were observed in the BALF from 2 days post-infection (2 dpi) (Fig. 1a). Each leukocyte population in the BALF was counted during 2 and 4 dpi, as the cell number on 1 dpi was quite small (Fig. 1b). The neutrophils were acutely accumulated with a peak on 2 dpi, and were reduced rapidly after 3 dpi. Macrophages increased significantly on 3 dpi and maintained the peak until 4 dpi. A small number of lymphocytes were also detected, but their increase was not observed during the infection. The nucleoproteins of propagated PR-8 virus were detected mainly in both bronchiolar epithelia and type II alveolar pneumocytes on 4 dpi (Fig. 1c). On 8 dpi, hyaline membranes were developed and detected in pulmonary alveoli (Fig. 1d). The infected mice progressed to death due to respiratory distress syndrome after 7–8 dpi with a short time from onset to final phase.

Expression profiles of claudin members during infection

To compare the alteration of claudin expression between uninfected and infected lung tissue, relative gene expression of all claudins (isotype 1–24 genes) was quantified with normalization by expression level of the internal standard gene. The mRNA levels of claudins 2 and 4 were

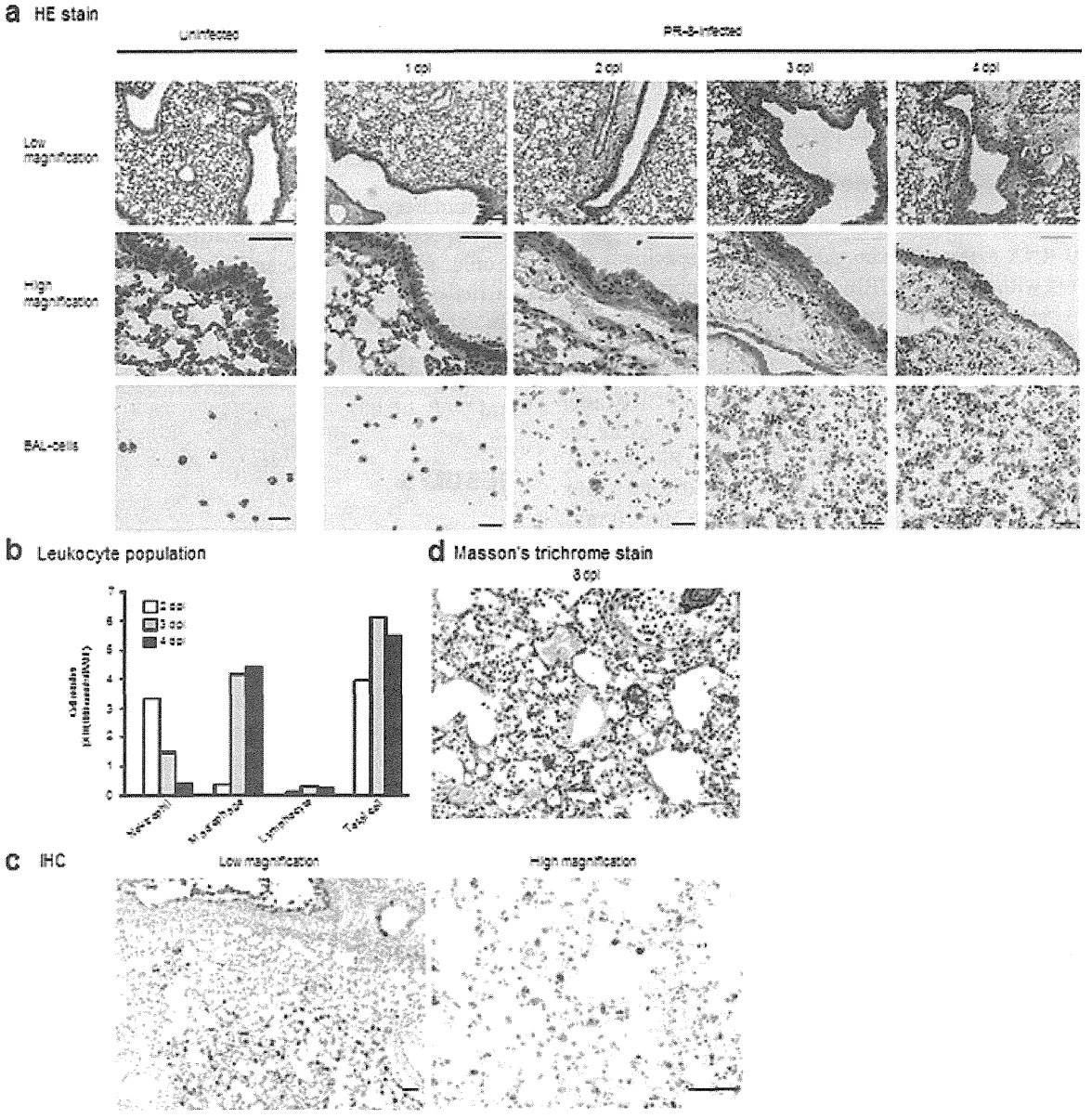

Fig. 1. Histopathologies of PR-8-infected lung. Micrographs are shown as representative data from more than three individuals. (a) HE staining and diff-quick staining modified from the Wright-Giemsa stain. Low magnification (upper panels, scale bar, 100 μm) and high magnification (middle panels, scale bar, 50 μm) of lung pathological images and Cytospin-prepared BAL cells (lower panels, scale bar, 50 μm) from BALF are shown. (b) Each leukocyte population infiltrated into the BALF during the infection. The cell number of neutrophils, macrophages, and lymphocytes in the BALF from 2 to 4 dpi is shown as the average of results from three individuals. (c) Immunohistochemistry for influenza virus A nucleoprotein (InfA-NP) on 4 dpi. The InfA-NP antigens were detected in bronchiolar epithelial cells and type II alveolar cells. Scale bars, 500 μm (left) and 50 μm (right), respectively. (d) Masson's trichrome staining of lung on 8 dpi. Hyaline membrane formations were observed on the alveolar walls. Scale bar, 50 μm.

increased, whereas the expression levels of claudins 6, 9, and 18–1 in the lung tissue were decreased by PR-8 infection (Fig. 2). There are no significant differences in expression level of other claudin isotypes (data not shown).

Cytokine proteins in BALF and their gene expression in lung tissue after infection

Production of IFN and stimulation of IRF were investigated in the pneumonia model. The production of IFN-α

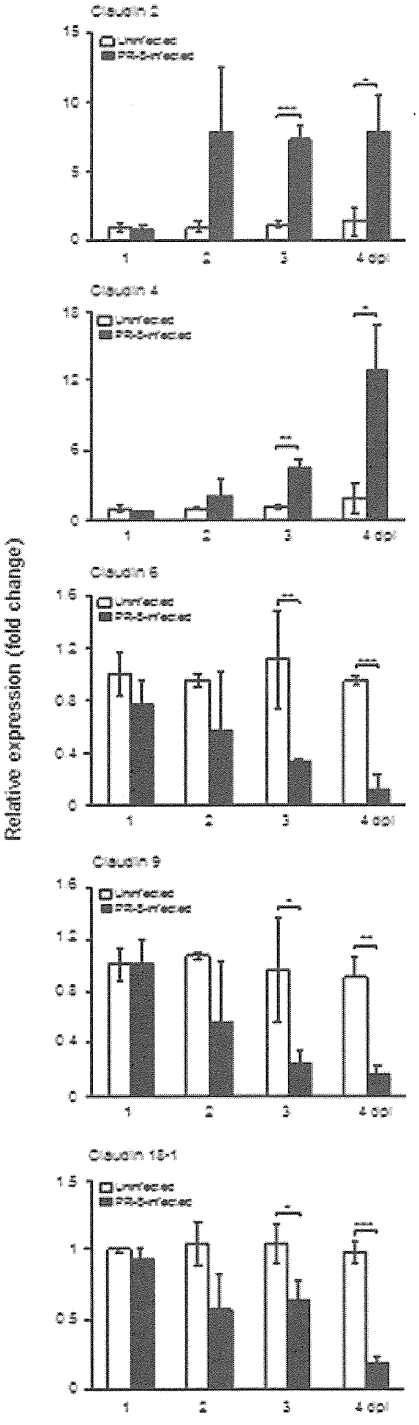

Fig. 2. Expression profiles of claudin genes during influenza virus pneumonia. Relative mRNA expressions of claudin in uninfected and infected lung with PR-8 at 1400 p.f.u. were examined by quantitative real-time PCR. The expression level of each claudin gene in lung tissue was calculated relative to GAPDH mRNA level. PR-8-infected and uninfected groups were composed of three mice. Data are shown as the mean ± SD of results from three individuals.*$P < 0.05$, **$P < 0.01$, and ***$P < 0.001$ (Student's t-test).

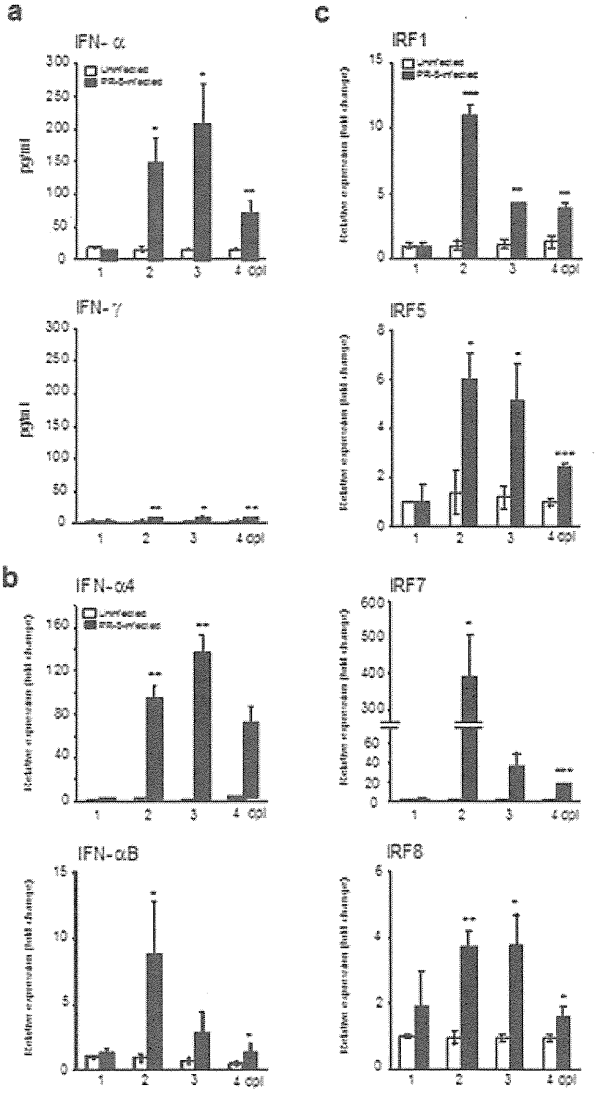

Fig. 3. Production and expression of IFN triggered by influenza virus infection. (a) Production of IFN in BALF in the infected lung with PR-8 at 1400 p.f.u. IFN-α and IFN-γ proteins in BALF from the uninfected and infected lung were measured by ELISA. Relative mRNA expression of IFN-α4 and αB subtypes (b), and IRF (c) in lung tissue measured by quantitative real-time PCR. The expression level of each gene was calculated relative to β-actin mRNA level. Each group was composed of three mice. Data in the figures are expressed as the mean ± SD of results from three individuals. *$P < 0.05$, **$P < 0.01$, and ***$P < 0.001$ (Student's t-test).

peaked in BALF on 3 dpi, whereas that of IFN-γ remained at lower level (Fig 3a). Among IFN-α subtypes, expressions of IFN-α4 and IFN-αB genes were enhanced in lung tissues by PR-8 infection (Fig. 3b). The expressions of IRF1, −5, −7, and −8 genes were also stimulated by the infection (Fig. 3c).

Production of 23 other kinds of cytokine proteins in BALF was exhaustively investigated in the model. Among

these cytokines tested here, IL-1α, IL-1β, IL-6, IL-12 p40, IL-13, TNF-α, G-CSF, and GM-CSF in addition to chemokines such as eotaxin, MIP-1α, and MIP-1β were elevated in BALF (Fig. 4a). In particular, KC (CXCL1), MIP-2 (CXCL2), RANTES (CCL5), and MCP-1 (CCL2) were remarkably released into BALF and the production level reached a peak sequentially between 2 and 4 dpi (Fig. 4b). We next quantitated mRNA expression of them in infected lung tissues (Fig. 4c). Their relative expression levels were well correlated with their protein profiles in BALF except for MCP-1, whose mRNA level peaked at 1 day. The protein productions of IL-2, IL-3, IL-4, IL-5, IL-9, IL-10, IL-12p70, and IL-17 in the BALF were at a notably low level in this model (data not shown). Cytokines and chemokines were also detected in plasma during the infection, but their production levels were lower than those in BALF, except for TNF-α and eotaxin (Figure S1). These findings indicate that a large quantity of KC, MIP-2, RANTES, and MCP-1 were produced in the early stage of influenza virus infection. The sequential production of these key chemokines seems operative for infiltration of each leukocyte population in the BALF during the infection.

Comparative analyses with MPO$^{-/-}$ mice

Neutrophils, in a reaction catalyzed by MPO, produce HOCl, which is reactive oxygen, a potent tissue injury factor (20–22). We therefore used a knockout mouse genetically lacking in the MPO gene, which has been described previously (17,18). Lung damage level, cytokine production, and viral expansion were compared between MPO$^{-/-}$ and wild-type mice during the infection.

MPO activity was undetectable in BALF of MPO$^{-/-}$ mice in comparison with that in wild-type mice during the infection (Fig. 5a). Histopathology of the lung suggested that disruption of pulmonary architecture in the lung from MPO$^{-/-}$ mice was less severe than that of wild-type (Fig. 5b). The concentration of total protein in the BALF of MPO$^{-/-}$ mice was lower than that of wild-type during the infection from 2 to 4 dpi (Fig. 5c). However, a survival difference between MPO$^{-/-}$ and wild-type mice was not observed (data not shown).

Viral load in the lung was examined in MPO$^{-/-}$ and wild-type mice by IHC on 4 dpi (Fig. 6a). Unexpectedly, the frequency distribution of viral nucleoproteins in MPO$^{-/-}$ mice was lower than that of wild-type mice. Quantitative analysis of viral nucleotides supported that the expression of the matrix 1 (M1) gene of PR-8 was suppressed in the lungs of MPO$^{-/-}$ mice relative to wild-type mice on 4 dpi (Fig. 6b).

To investigate the pathophysiological difference between MPO$^{-/-}$ and wild-type mice with ARDS, cytokine proteins in BALF were quantitated and compared in the two mouse strains (Fig. 7). Among 23 kinds of cytokines/chemokines, the production of MIP-1β production was increased, whereas GM-CSF was suppressed in the BALF of MPO$^{-/-}$ mice, compared with that in wild-type mice on 4 dpi (Fig. 7a). There were no significant differences in the production level of other cytokines between both mouse strains (data not shown). Gene expression of claudins in the lung tissue was also investigated between MPO$^{-/-}$ and wild-type mice during the infection (Fig. 7b). Claudins 2 and 4 did not show a significant difference in expression level between both strains on 4 dpi. In contrast, expression of claudins 9 and 18–1 was higher in the lung of MPO$^{-/-}$ mice than in that of wild-type mice (Fig. 7b).

DISCUSSION

In the present study, high-dose inoculation of PR-8 virus into BALB/c mice resulted in severe pneumonia with recruitment of leukocytes and disruption of alveolar walls, followed by formation of hyaline membranes. This severe pneumonia satisfies the criteria for fulminant ARDS with diffuse alveolar damage and hyaline membrane formation, leading to death in a short time from onset. This fulminant severe pneumonia caused by PR-8 virus infection is an experimental mouse model for fulminant ARDS.

In the model, lung damage was histologically observed in parallel with enhancement of claudins 2 and 4 and suppression of claudins 6, 9, and 18–1 expression. Claudins 2 and 4 are known to be associated with ALI (7,8), whereas the relation of claudins 6, 9, and 18–1 to lung injury has never been elucidated. In ALI, TNF-α, IL-6, and IL-1β increase the production of claudins 2 and 4 and affect TJ barrier function (8,9). Similar conditions were observed in our model with enhancement of TNF-α, IL-6, and IL-1β production in the BALF. It is reported that blockage of claudin 4 function causes TJ leak, resulting in pulmonary edema (8). These observations suggest that augmentation of claudins 2 and 4 by proinflammatory cytokines may protect from lung damage by influenza pneumonia.

During the infection, IFN-α, but not IFN-γ, was significantly produced in the BALF. IFN-α exerts anti-influenza virus activity in the acute phase of the infection (23–26), and IFN-α4 and IFN-αB are stimulated by the infection with A/NWS/33 (A/H1N1) influenza virus *in vitro* (23–26). Our study showed that expressions of these isotypes were promoted by the infection. The *in vitro* findings of both isotypes are supported by our data, which are the first recorded under *in vivo* conditions. These IFN-α subtypes most likely play protective roles in influenza virus infection. By contrast, it has been reported that IFN-γ is mainly produced 6–8 days after influenza virus infection

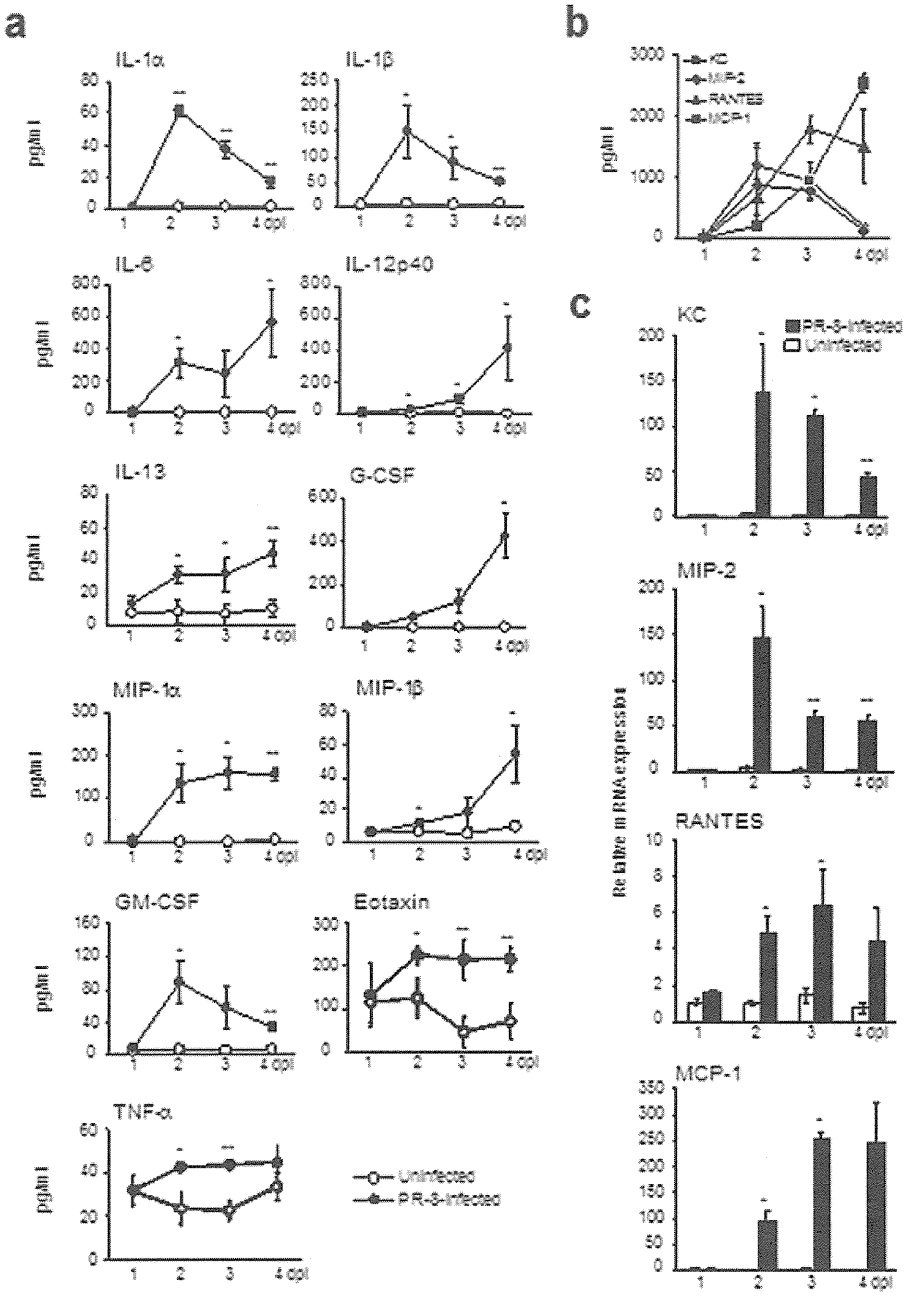

Fig. 4. Production and expression of cytokines/chemokines during influenza virus infection. (a) Production of cytokines/chemokines in BALF in uninfected and infected mice with PR-8 at 1400 p.f.u. (b) The dominant four types of chemokines sequentially produced in BALF by the infection. (c) Relative mRNA expression of the dominant chemokines in the infected lung tissues. The expression level of each gene in lung tissue was calculated relative to β-actin mRNA level. Each group was composed of three mice. Data in the figures are expressed as the mean ± SD of results from three individuals. $^{*}P < 0.05$, $^{**}P < 0.01$, and $^{***}P < 0.001$ (Student's *t*-test).

in both *in vivo* and *in vitro* conditions (14,24,27). In our fulminant ARDS model, IFN-γ may not be involved in the early phase of the infection. IRF members were up-regulated by influenza virus infection in the present study. Indeed, it has been reported that IRF1 and IRF7 mediate type I IFN production in influenza virus infection (28–30). IRF5 and IRF8 positively regulate type I IFN production after infection with Newcastle disease virus (31,32). We

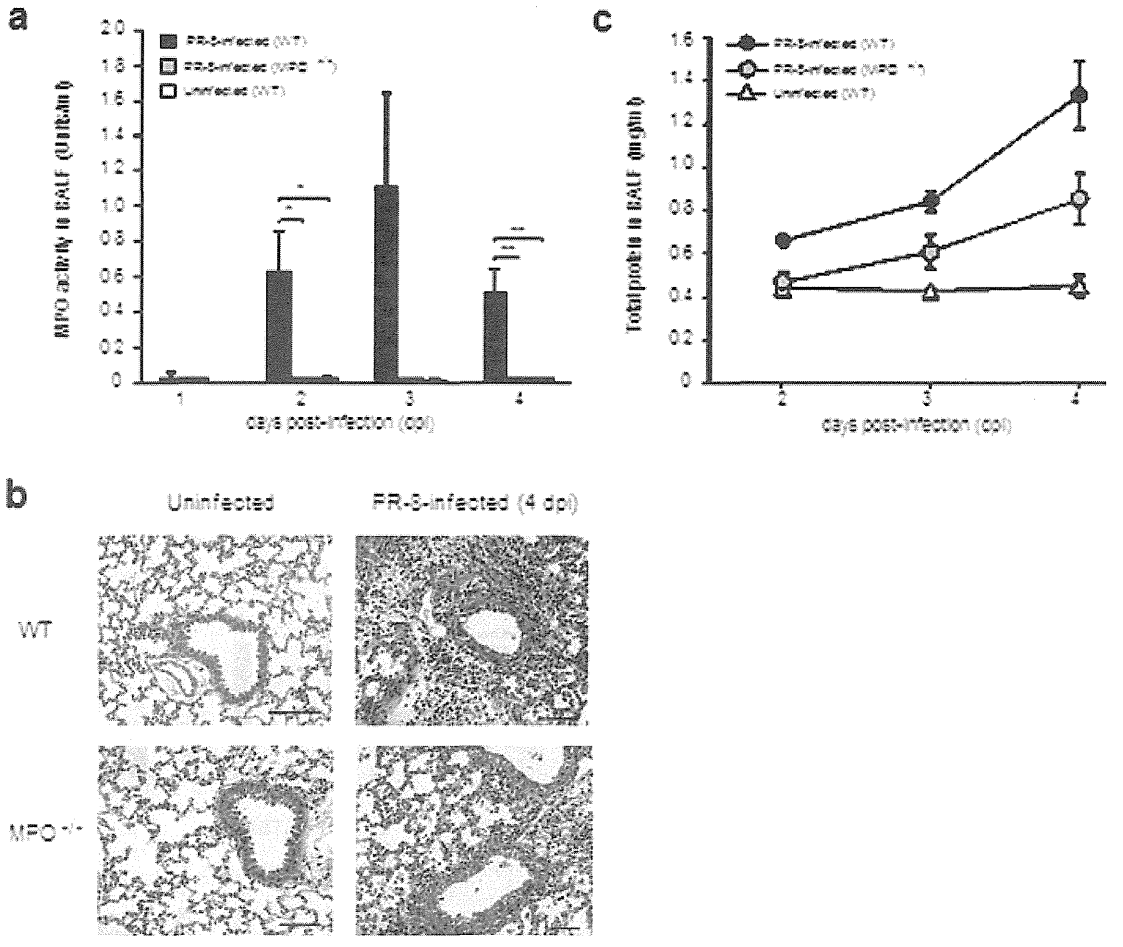

Fig. 5. Comparative analyses between MPO$^{-/-}$ and wild-type mice in influenza virus infection. (a) MPO activity in lung BALF of each mouse group infected with PR-8 at 1400 p.f.u. The activities were measured on 1, 2, 3, and 4 dpi, but data of MPO$^{-/-}$ mice on 1 dpi are absent. Each point is shown as the mean ± SD of results from three individuals. *$P < 0.05$ and **$P < 0.01$ (Student's *t*-test). (b) Histopathologies in lung tissue from wild-type and MPO$^{-/-}$ mice. Mouse groups were infected with PR-8 at 1400 p.f.u., and inflammation and injury levels in the lung were compared between MPO$^{-/-}$ and wild-type mice. Histological data are shown as representative results from more than two individuals. Scale bars, 100 μm. (c) Efflux of total BALF protein of MPO$^{-/-}$ and wild-type mice during the infection. The concentration of protein in the BALF of wild-type, MPO$^{-/-}$, and uninfected mice was measured on 2, 3, and 4 dpi. Each point is shown as the mean ± SD of results from three individuals.

first showed that IRF5 and IRF8 expressions were elevated during influenza virus infection. These IRF may regulate production of IFN-α subtypes in the influenza virus infection.

Chemokines, KC, MIP-2, RANTES, and MCP-1, were significantly released into BALF by the infection. Among them, KC and MIP-2 were first expressed and produced on 2 dpi. During this time, a large number of neutrophils were observed in the lung, which is also supported by the detection of high MPO activity. Both KC and MIP-2 are chemoattractants for neutrophils in lung inflammation (33). Therefore, KC and MIP-2 produced in the lung play chemotactic roles in neutrophil recruitment for pneumonia at the early stage of influenza virus infection.

Following the production of KC and MIP-2, RANTES was subsequently produced in the BALF during 3 and 4 dpi. This chemokine is produced by bronchial epithelial cells after influenza virus infection *in vitro* and shows strong chemotactic activity for eosinophils (34). The influx of eosinophils is involved in acute allergic inflammation such as asthma, and it has recently been reported that asthmatic inflammatory reaction is induced by viral infection (35–37). Although the precise role of eosinophils in influenza virus infection is unclear, recruited eosinophils may exacerbate the inflammation.

Our observation of MCP-1 production, which leads to macrophage infiltration, agrees with the previous literatures (38,39). Macrophages in the lung and BALF